

Mediterranean Forecasting System: An improved assimilation scheme for sea-level anomaly and its validation

By S. DOBRICIC^{1*}, N. PINARDI^{1,2}, M. ADANI¹, A. BONAZZI¹, C. FRATIANNI¹ and M. TONANI¹

¹*Istituto Nazionale di Geofisica e Vulcanologia, Italy*

²*University of Bologna, Italy*

(Received 23 May 2005; revised 16 January 2006)

SUMMARY

The assimilation of satellite and *in situ* data in the Mediterranean Forecast System (MFS) is based on an optimal interpolation scheme which uses empirical orthogonal functions (EOFs) to represent vertical modes of the background-error correlation matrix. In this study we present a new methodology to estimate, and the calculation of, these multivariate EOFs. The new EOFs are considered time and space varying (seasonal time-scales and subregional). They examine the vertical-error cross-variance between temperature, salinity, barotropic stream function and sea-level anomaly. These EOFs are used to assimilate four years of along-track sea-level anomaly data. The validation of MFS analyses and forecasts using the assimilation system diagnostics and the comparison with independent observations show that, in relation to an old operational scheme which was using only one EOF, the use of several multivariate EOFs significantly improves the accuracy of analyses and forecasts in the Mediterranean.

KEYWORDS: Data assimilation Operational oceanography Physical oceanography

1. INTRODUCTION

The Mediterranean Forecasting System (MFS) is an operational oceanographic system in the Mediterranean Sea which involves the work of 48 institutes from 15 countries. Its activity combines observations, data collection, data assimilation, oceanographic forecasts and the ecosystem modelling and forecasts (Pinardi *et al.* 2003). In order to assess the whole variability of different oceanographic conditions in the Mediterranean, the MFS is composed of the large-scale observing and forecasting system and several nested regional and local systems along coastal areas.

One of the major components of the MFS is the data assimilation system of the basin-scale model described in Demirov *et al.* (2003). There are three types of observations which are operationally assimilated on the basin scale: the sea surface temperature (SST) fields objectively analysed on the MFS basin-scale model grid, the sea-level anomaly (SLA) along-track observations (Le Traon *et al.* 1998) and temperature vertical profiles. While the SST and the SLA observations are obtained remotely by satellites, temperature vertical profiles are measured *in situ* by expendable bathythermograph (XBT) instruments from ships as available (Manzella *et al.* 2001). The SST assimilation consists of correcting surface heat flux by a relaxation of the numerical model surface-layer temperature towards the observed SST. The SLA and XBT datasets are assimilated using the System for Ocean Forecasting and Analysis (SOFA) optimal interpolation scheme (De Mey and Benkiran 2002).

In a multivariate assimilation scheme the background-error covariance should spread corrections from observations to model variables in a statistically and dynamically consistent way. Therefore, its specification is one of the most important parts of any data assimilation system (e.g. Derber and Bouttier 1999). Starting from some initial estimate, in the 4D-Var assimilation, the background-error covariance matrix is modified implicitly using the tangent linear model and its adjoint (e.g. Talagrand and Courtier 1987), while in applications with the Kalman filter it is propagated by the linear model

* Corresponding author: Istituto di Geofisica e Vulcanologia, Via Creti 12, 40128 Bologna, Italy.
e-mail: dobricic@bo.ingv.it

and updated by the estimate of the model error (e.g. Todling and Cohn 1994). On the other hand, in 3D-Var and optimal interpolation assimilation schemes the a priori estimate of the background-error covariances is not changed during the assimilation period. This approach requires two major assumptions: (i) the background-error correlations do not change due to the assimilation of data, although they can slowly change temporally (e.g. seasonally); (ii) we precisely know their structure and magnitude in advance. In multivariate assimilation schemes it is difficult to fully satisfy both assumptions. The fulfilment of these assumptions is especially important in the MFS assimilation system which uses a relatively large number of surface observations of SLA to propagate the analysis corrections into deep layers of the ocean. Therefore, we can expect that a more accurate estimate of the background-error covariances will have an important influence on the quality of the MFS analysis.

The purpose of this study is to describe recent modifications of the background-error covariance matrix in the MFS assimilation system for SLA and to quantitatively compare the performance of the new assimilation scheme with the old one. The modifications consist in changing the original background-error covariance matrix description, which used only one vertical multivariate error empirical orthogonal function (EOF), with a new formulation which considers a relatively large number of vertical modes depending on the geographical region and season.

Section 2 describes the MFS assimilation system. In section 3 we describe the method to calculate the new background-error covariance matrix, while in section 4 we compare the results of the new assimilation scheme with those of the old operational scheme. The discussion and conclusions are given in section 5.

2. THE MFS ASSIMILATION SYSTEM

The ‘old’ operational MFS assimilation scheme, called MARK2, uses the SOFA optimal interpolation scheme (De Mey and Benkiran 2002) and is described in Demirov *et al.* (2003). This is an approximation of the Kalman filter with the analysis calculated from the formula:

$$\mathbf{x}_a = \mathbf{x}_b + \mathbf{K}\{\mathbf{y} - H(\mathbf{x}_b)\}, \quad (1)$$

where \mathbf{x}_a is the analysis state vector, \mathbf{x}_b is the background state vector, \mathbf{y} is the vector of observations, $H(\cdot)$ is the nonlinear operator mapping the state vector to observations, and \mathbf{K} is obtained from:

$$\mathbf{K} = \mathbf{B}\mathbf{H}^T(\mathbf{H}\mathbf{B}\mathbf{H}^T + \mathbf{R})^{-1}, \quad (2)$$

where \mathbf{B} is the background-error covariance matrix, \mathbf{R} the observational-error covariance matrix and \mathbf{H} the linearized observational operator. The background-error covariance matrix \mathbf{B} is approximated assuming that horizontal and vertical-error covariances are independent:

$$\mathbf{B} = \mathbf{S}^T\mathbf{B}_r\mathbf{S}. \quad (3)$$

The matrix \mathbf{S} contains vertical-error covariance EOFs while $\mathbf{B}_r = \mathbf{\Lambda}^{1/2}\mathbf{C}\mathbf{\Lambda}^{1/2}$ is composed by horizontal covariances in \mathbf{C} (modelled as Gaussian functions) for each vertical EOF and eigenvalues of the vertical-error covariances in $\mathbf{\Lambda}$. Typically only the most significant number of vertical EOFs are used in order to reduce the cost of computations and to filter the background-error correlation matrix from modes that do not account for the largest part of the variance (i.e. their eigenvalues are small).

The observations of SLA and XBT, giving vertical temperature profiles, are assimilated once a week using two different vertical-error correlation matrices in (3). The use

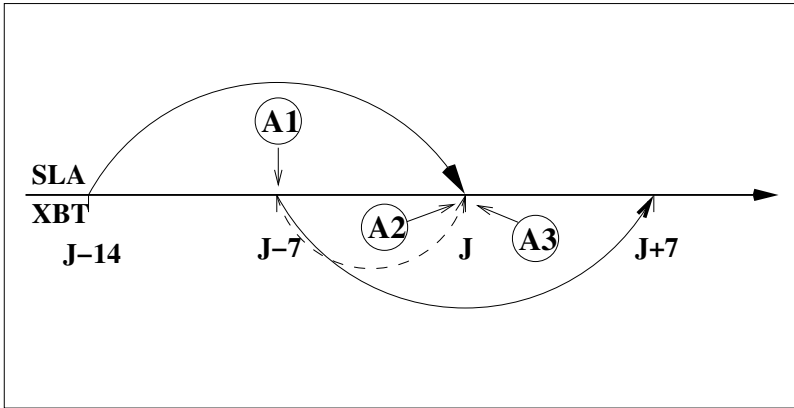


Figure 1. The analysis cycle in the MFS. The horizontal line indicates the time in days and J is the starting day of the forecast. The analysis A1 uses only the SLA dataset and analyses A2 and A3 only the XBT data, starting from the A1. The analysis A3 substitutes the analyses A2 after the forecast is done. In A3, like in A2, the background model integration starts from A1. A3 uses the same observations as A2 during the week between J-7 and J but it also uses the observations available in the following week. In this way each observation is assimilated only once.

of different background correlation matrices requires the separate assimilation of each dataset. The analysis time window is taken to be two weeks and the analysis is done at the central time (Fig. 1). When the analysis A1 in Fig. 1 is done using only SLA observations, the next analysis is made using only observations of vertical temperature profiles (A2 and A3 in Fig. 1). In this way all observations are assimilated once in the system using two background-error covariance matrices. However, in the operational application it is necessary to make an analysis only knowing the previous week's data in order to launch the forecast: thus the analysis A2 is done temporarily (see Fig. 1) and one week later the analysis A2 is substituted by the central analysis A3, made using observations from two weeks.

The vertical modes of the background-error correlation matrix for the assimilation of vertical temperature profiles are calculated from historical Conductivity–Temperature–Depth (CTD) profiles of temperature and salinity (Sparnocchia *et al.* 2003). On the other hand, the MARK2 SLA assimilation uses a single vertical EOF mode calculated from the water mass characteristics of the western Mediterranean (De Mey and Benkiran 2002; Demirov *et al.* 2003). In the top levels, above 120 m depth, these EOF values are set to zero in order to avoid the errors in the representation of the high variability of temperature and salinity fields in the mixed layer using only one EOF for the whole Mediterranean. In this study we will propose a MARK3 assimilation system for SLA assimilation which uses temporally and regionally varying EOFs.

The observational operator for SLA is based on the assumption that in the geostrophic limit the background error in SLA reflects errors in temperature, salinity and velocity fields in the water column. It uses the formula of Pinardi *et al.* (1995) to link the correction of the surface elevation with corrections of the barotropic stream function, temperature and salinity in an ocean with the constant depth H :

$$\delta\eta = \frac{f\delta\Psi}{gH} - \frac{1}{\rho_0 H} \int_{-H}^0 \left(\frac{\partial\rho}{\partial T}\delta T + \frac{\partial\rho}{\partial S}\delta S \right) (z+H) dz, \quad (4)$$

where z is height and g is the acceleration due to gravity. In (4) $\delta\eta$, $\delta\Psi$, δT and δS are corrections of the surface elevation, barotropic stream function, temperature and

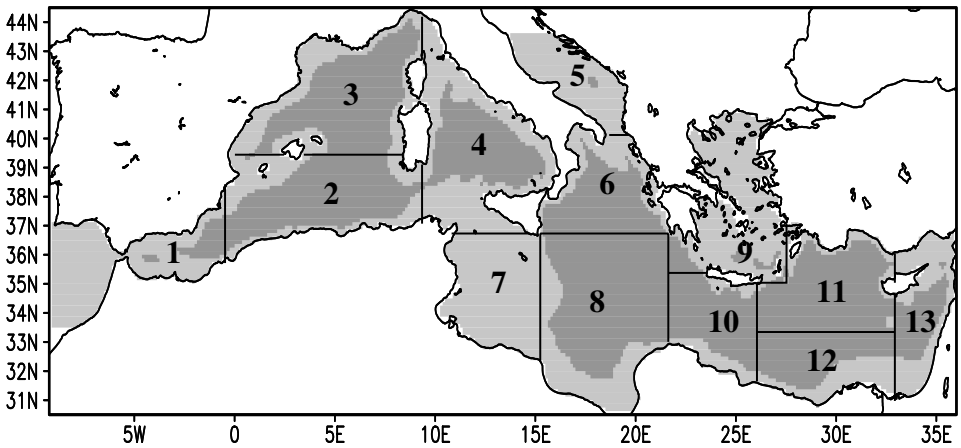


Figure 2. The MFS basin-scale model domain (light grey) and the area in which SLA observations are assimilated (dark grey). Also shown are the position and boundaries of 13 geographical regions used for the calculation of different vertical error EOFs.

salinity, respectively. The density $\rho(T, S)$ is linearized around its background value, and H is the constant depth of 1000 m. The value of 1000 m is empirically determined by noticing that the diagnosed sea surface elevation field is very similar to that obtained by the inversion of the full surface pressure equation (not shown). However, this operator restricts the SLA assimilation only to areas of the Mediterranean which are at least 1000 m deep. Figure 2 shows the areas in which the SLA data is assimilated given this choice.

The assimilation of SST data is performed by the relaxation of the temperature in the top model layer towards the weekly objective analysis of SST. The coefficient of relaxation corresponds to the correction of surface heat fluxes of 40 W m^{-2} for a difference between model and data of 1 degC.

The background fields are produced by an implementation of the Modular Ocean Model-MOM to the Mediterranean Sea (Demirov and Pinardi 2002; Pinardi *et al.* 2003). The model has a horizontal resolution of 0.125° and 31 levels in the vertical. The atmospheric forcing is calculated in an interactive way (Castellari *et al.* 1998) using atmospheric analyses from the European Centre for the Medium range Weather Forecast (ECMWF), and the top model layer salinity is relaxed towards monthly mean climatology. The model started the assimilation on 31 August 1999. The initial state was produced by taking the January simulation from a climatological experiment forced with climatological surface fluxes for seven years and then, starting from 1 January 1997, forced with six-hourly analyses from ECMWF.

3. CALCULATION OF THE NEW BACKGROUND-ERROR COVARIANCE MATRIX FOR SLA ASSIMILATION

The single EOF used in MARK2 to represent \mathbf{S} in (3) cannot represent the whole variability of the vertical structure of the background-error covariance in the Mediterranean. This problem is especially important when we compare the water mass characteristics of the western and the eastern Mediterranean. While in the western Mediterranean the vertical structure of the background-error covariances is significantly influenced by the position and depth of the modified Atlantic water, in the eastern

Mediterranean the errors in the temperature field at the surface become more important. Therefore, we could expect that the single EOF used in MARK2 does not propagate correctly the two-dimensional corrections from SLA residuals into three-dimensional corrections of temperature and salinity in all parts of the Mediterranean Sea and that this problem could be especially pronounced in the eastern Mediterranean.

In order to create a more accurate vertical structure of the background-error covariance matrix we decided to compute separate sets of EOFs in different geographical parts of the Mediterranean. In particular, the EOFs are calculated for the combined temperature, salinity, stream function and sea-surface-elevation statistics, dividing the Mediterranean Sea into 13 regions (see Fig. 2). The fields used for the computation of EOFs originate from an interannual simulation ranging from 1993 to 1999. The seasonal and geographical grouping is made in order to select vertical profiles which have similar water mass properties (Sparnocchia *et al.* 2003). Inside each region, only the grid points deeper than 1000 m are selected and each water column is truncated at 1000 m. The daily averaged model field anomalies in each geographical region resulted in a minimum dataset of more than 600 multi-variate profiles which were sufficient to calculate EOFs.

Every temperature and salinity profile, stream function and sea-surface-elevation value from the model are taken to form a state matrix \mathbf{X} containing $2m + 2$ non-dimensional vectors (where m is the number of model vertical levels above the depth of 1000 m):

$$\mathbf{X} = \left(\frac{\delta\eta}{\sigma_\eta}, \frac{\delta\Psi}{\sigma_\psi}, \frac{\delta T_1}{\sigma_T}, \dots, \frac{\delta T_m}{\sigma_T}, \frac{\delta S_1}{\sigma_S}, \dots, \frac{\delta S_m}{\sigma_S} \right), \quad (5)$$

where σ_η , σ_ψ , σ_T and σ_S represent the standard deviation of corresponding fields, and δ indicates the difference between the daily averaged value and temporal mean for each season. Each vector composing (5) is a time series of daily values.

The S modes used in (3) are then computed by the singular value composition of \mathbf{X} , i.e.

$$\mathbf{X} = \mathbf{S}\mathbf{A}^{1/2}\mathbf{V}^T. \quad (6)$$

Initial tests showed that the dimensional scaling in (5) was not sufficient to obtain EOFs which were different between the case with the state vector that included all four variables and the one calculated only from temperature and salinity. This result can be explained by the fact that in this case the relative contribution given by the stream function or by the surface elevation on the matrix (5) is small with respect to temperature and salinity. Therefore, the matrix is dominated by the covariance modes of temperature and salinity.

In order to create EOFs independent of space geometry, i.e. number of levels, thickness of levels and in general the grid spacing, we decided to multiply the state vector \mathbf{X} (defined in (5)) by a metric factor matrix \mathbf{g} (North *et al.* 1982) whose diagonal elements are:

$$\mathbf{g} = \text{diag} \left(1, 1, \frac{\Delta z_1}{H}, \dots, \frac{\Delta z_m}{H}, \frac{\Delta z_1}{H}, \dots, \frac{\Delta z_m}{H} \right), \quad (7)$$

where the Δz are the model layer thicknesses and H is the constant model depth of 1000 m. Although it is well known that the multiplication by the layer thickness results in different EOFs, the consequences of this scaling go far beyond this fact. As we can see from (4), sea surface elevation and barotropic stream-function errors are approximately given by vertically integrated errors in temperature and salinity fields. Therefore, we can expect that thicker layers with the same variance of temperature and salinity should have a proportionally larger influence on the errors in surface elevation and barotropic stream

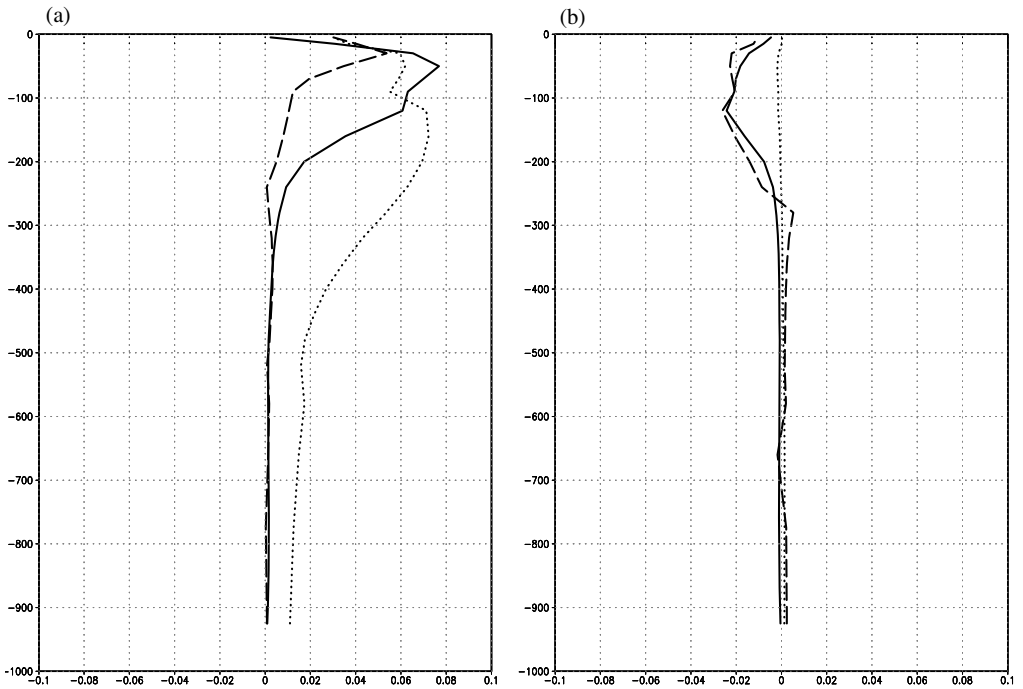


Figure 3. Vertical structure of the first vertical-error EOF (height in metres) in S (see text) for (a) temperature ($^{\circ}\text{C}$), and (b) salinity (PSU), in regions 1, 8 and 11 multiplied by their explained variance and for summer. Region 1 is represented by the full line, region 8 by the dashed line and region 11 by the dotted line.

function. This means that temperature and salinity multiplied by the layer thickness more closely represents the real physical relationships between the temperature and salinity fields and changes in the sea surface elevation. The EOF modes are calculated as in (6), but with \mathbf{X} scaled by the metric factor matrix (7). To construct \mathbf{S} we need to retrieve the EOFs in the physical space and then the modes are re-scaled by the inverse of (7).

Figure 3 shows the vertical structure of the first EOF of the temperature and salinity variability (assumed to approximate the vertical background error) computed for regions 1, 8 and 11 (shown in Fig. 2) in summer. In regions 1 and 8 the first EOF of salinity has a similarly important variation like the first EOF of temperature. On the contrary, in the region 11 the first temperature EOF has a significantly larger magnitude than the first salinity EOF. We can explain the difference in the vertical structure of the first EOF by the fact that regions 1 and 8 have a relatively large variance in salinity between the modified Atlantic water and the Levantine subsurface water layers, while in region 11 this variance is attenuated due to mixing during the eastward advection of the Atlantic waters, and the largest water mass variance is due to temperature differences.

The structure of the error vertical covariance matrix constructed from (5) as \mathbf{XX}^T in region 1 and for summer is shown in Fig. 4. We can see that temperature and salinity at all levels are correlated with the surface elevation. The maximum correlation is approximately at the bottom of the mixed layer where temperature and salinity have the largest variance. Also, the same levels show the largest correlation between the temperature and salinity fields. A similar vertical correlation structure is also obtained in all other regions and seasons (not shown). The largest variance and correlation magnitudes are

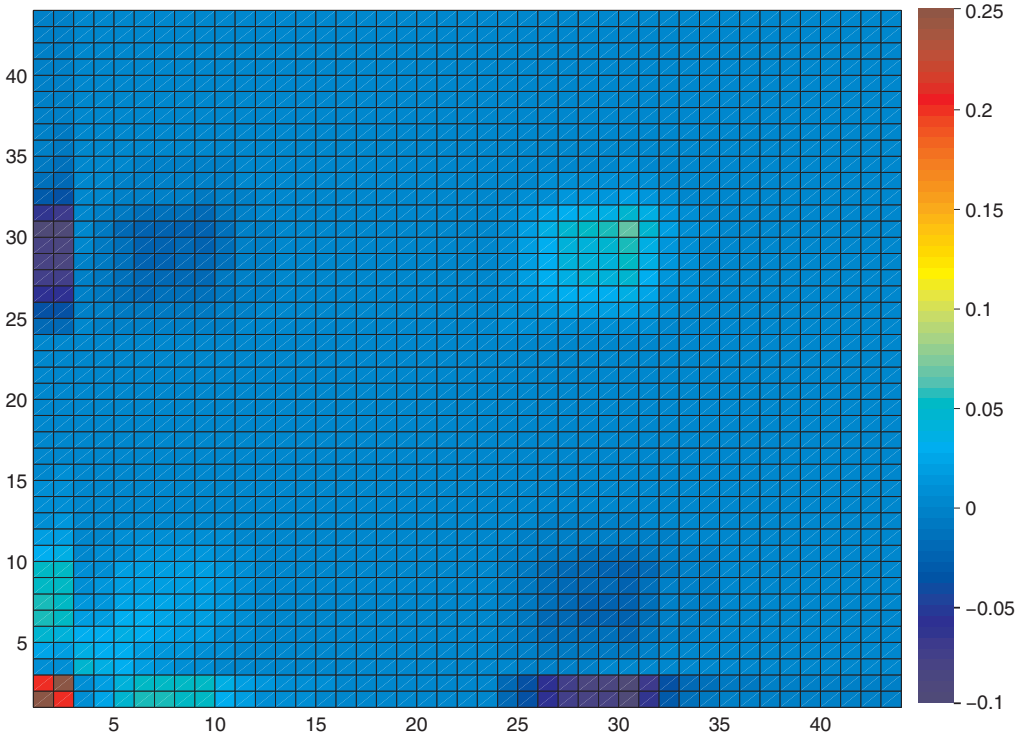


Figure 4. The vertical correlation matrix \mathbf{XX}^T for the region 1 in summer. Starting from the bottom left corner, the first element corresponds to the surface elevation correlation, the second to barotropic stream-function correlation and then there are 21 levels with temperature and 21 levels with salinity. All values are scaled by their standard deviations as explained in (5) and by the trace of \mathbf{XX}^T in order to represent them with comparable magnitudes.

placed around the bottom of the mixed layer, because there the variance of temperature and salinity is the largest. For the temperature field this result is consistent with the hypothesis that the background-error variance is proportional to the magnitude of the vertical gradient of the temperature (e.g. Behringer *et al.* 1998). In fact, it was noticed that the maximum of the temperature variance was placed at the maximum of the mean vertical temperature gradient (not shown). Furthermore, we can see in Fig. 4 that the maximum of the salinity error variance is positioned deeper than the maximum of the temperature error variance. It was noticed that this depth coincided with the maximum of the mean vertical gradient of the salinity field (not shown). This indicates that the salinity error variance is the function of the vertical gradient of the salinity field, just like the the temperature error variance is the function of the mean vertical gradient of the temperature field. The spatial and seasonal variability of the position of the bottom of the mixed layer further confirms our initial hypothesis that it is necessary to have a seasonally and spatially variable representation of the background-error covariance matrix in order to accurately propagate in vertical corrections due to the SLA data assimilation in the Mediterranean.

In order to decide how many EOFs were sufficient to represent the vertical background-error covariance matrix, we reconstructed individual vertical profiles of temperature and salinity. This method differs from the usual one because of scaling given by \mathbf{g} . In fact, in the scaled space, 10 EOFs were enough to reproduce the vertical

TABLE 1. SENSITIVITY EXPERIMENTS DIFFERENCES. MARK2 IS THE OLD OPERATIONAL SCHEME AND REPRESENTS THE REFERENCE EXPERIMENT. EXP4 LABELLED MARK3 IS THE NEW OPERATIONAL SCHEME.

Experiment name	Number of regions	Number of EOFs	Variables
MARK2	1	1	Ψ, T, S
Exp2	13	20	Ψ, T, S
Exp3	13	10	Ψ, T, S
Exp4/MARK3	13	20	η, Ψ, T, S

See text for explanation of symbols.

scaled profiles of temperature and salinity, since the sum of the first 10 eigenvalues gives about 99% of the explained variance. However, going back to the physical space, by rescaling the EOFs at each level, the reconstruction needs to have at least 20 EOFs to reach an error of 0.01 degC for temperature and 0.01 PSU units for salinity. Therefore, we have decided to use 20 EOFs in the new formulation of the background-error correlation matrix for the SLA assimilation. The usage of 20 EOFs reduce the number of original vertical modes by approximately 2. Furthermore, we have performed a sensitivity experiment with 10 EOFs which is explained in the next section.

4. VALIDATION OF THE NEW ANALYSIS SCHEME

The influence of the new background-error covariance matrix modes on the quality of the analyses was evaluated by several sensitivity experiments. Sensitivity experiments contrasted by the different specification of several parameters of the new assimilation scheme are listed in Table 1.

Initial experiments with a duration of few months showed relatively large differences between the reference experiment MARK2 and experiments with the new background-error correlation matrices. The results of the most complex Exp4, which applies 20 quadrivariate EOFs, differ from Exp2, which applies trivariate EOFs, in terms of the magnitude of corrections, with the corrections having a slightly smaller magnitude in the experiment Exp4 (not shown). Similarly, Exp3 which used 10 trivariate EOFs, resulted in corrections with slightly smaller magnitude than those obtained with 20 trivariate EOFs in Exp2 (not shown). From these intercomparisons, however, we could not unequivocally evaluate which set of EOFs gave superior assimilation results. Based mainly on arguments from the last paragraph in section 3, we have arbitrarily decided to choose 20 quadrivariate EOFs for the MARK3 experiment.

The comparison experiment between MARK2 and MARK3 covered the period from September 1999 to May 2004. A relatively long period for the comparison between two assimilation systems gives the possibility to statistically compare the performance of the assimilation schemes during all seasons and with a large variety of atmospheric forcing conditions.

One year after the beginning of the assimilation, differences appeared between the two assimilation schemes, which were systematically present throughout the rest of the period of the comparison. Figure 5 shows the sea surface elevation estimated by MARK2 and MARK3 one year after the beginning of the assimilation. We can see that large-scale features in both experiments give a relatively similar result and correctly depict major structures of gyres and large currents. For example, by comparing with Fig. 1 in Pinardi and Masetti (2000) we can see that both experiments correctly simulate the general path of the Algerian current, the inflow of the Atlantic Stream into the Ionian south of Sicily, the flow of the Atlantic Stream along the north-eastern African coast, and

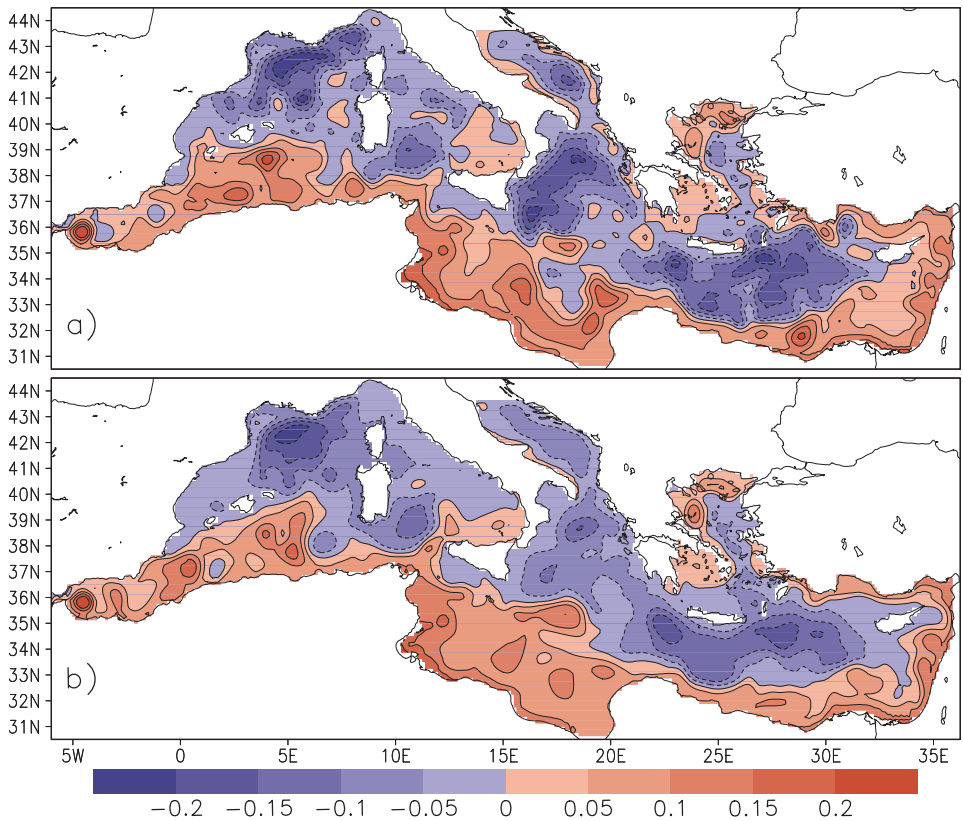


Figure 5. Sea-surface-elevation (cm) fields for 5 September 2000: (a) Experiment MARK2 and (b) Experiment MARK3 (see Table 1). These are snapshots approximately one year after the start of the assimilation (31 August 1999).

cyclonic circulations in the Levantine, the Adriatic and the western Mediterranean. On the other hand, there is a significant difference in the intensity of the surface circulation indicated by the gradient of the sea surface elevation field. The sea surface elevation gradients in MARK2 are more intense than in MARK3 indicating a stronger surface flow. Furthermore, MARK2 shows smaller-scale eddies, especially in the northern part of the Mediterranean.

The same type of differences between sea-surface-elevation fields simulated by the two experiments were obtained throughout a four-year-long period of the assimilation (not shown). Without a comparison with independent observations, these differences in the results do not indicate which assimilation scheme gives a better result, but we can conclude that large-scale features in surface analyses produced by two experiments are relatively similar. This conclusion could be expected, because sea surface elevation analysis fields are obtained from directly observed SLA data which are available with a relatively high temporal frequency and spatial resolution. However, it should be noticed that MOM is a rigid-lid model with the background sea-surface-elevation fields diagnostically calculated by inverting the Laplacian of the surface pressure. As a consequence, in MOM we only correct temperature, salinity and barotropic stream-function fields. However, the corrections are done in a way to reduce the residuals between diagnosed background sea-surface-elevation fields and SLA observations. Therefore,

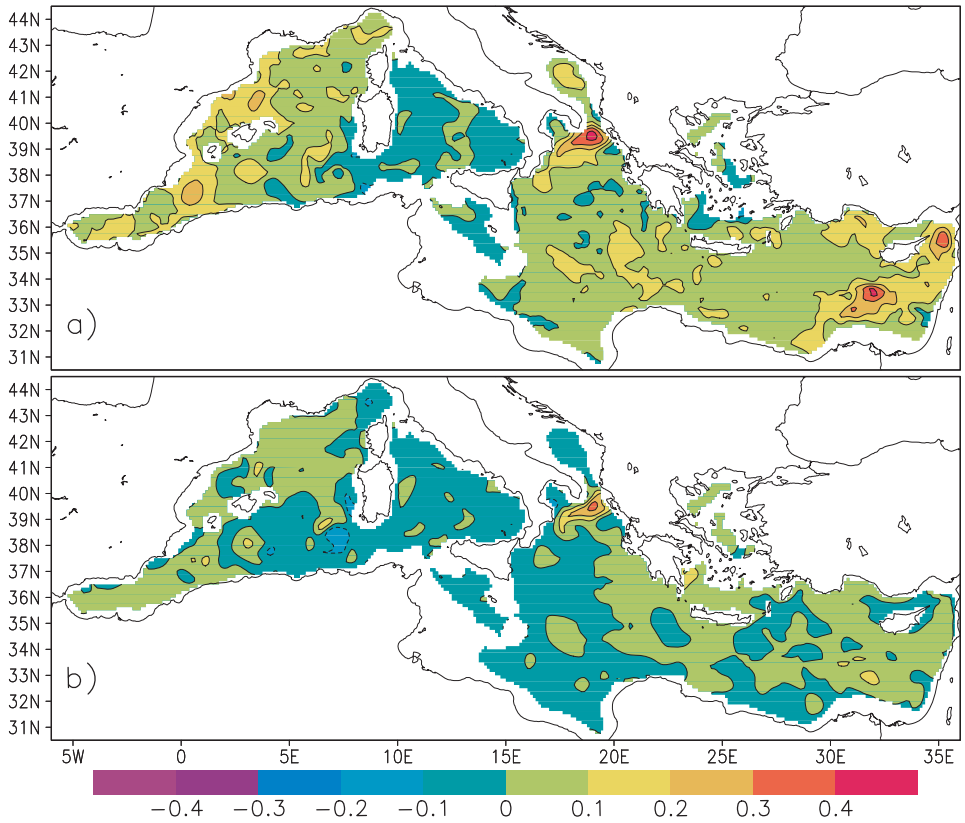


Figure 6. Difference between salinity on 5 September 2000 and 7 September 1999 at the depth of 350 m (PSU): (a) Experiment MARK2 and (b) Experiment MARK3.

sea-surface-elevation corrections depend mainly on residuals and less on the structure of the background-error correlation matrix and we can explain the large-scale similarity between the two experiments by the fact that they assimilated the same set of SLA observations.

On the other hand, we can expect that the change in the background-error correlation matrix will mostly influence the correction of fields that are not directly observed. In the case of the SLA assimilation these fields are temperature, salinity and the barotropic stream function. Figure 6 shows the difference between the salinity at the depth of 350 m on 5 September 2000 simulated by the two experiments and the initial salinity on 31 August 1999. Now we can see that MARK3 gives a result which is quite different from that of MARK2. In MARK2 there is a clear drift of the salinity towards higher values especially in the eastern Mediterranean. At the same time in MARK3 the drift is smaller if not absent. The salinity is higher in some areas and lower in others, showing a wave-like adjustment without large-scale drifts. The salinity drift in MARK2 was evident throughout the five-year-long comparison period, and in 2004, after the full period of comparison, the salinity at deep layers in MARK2 reached unrealistic values, while MARK3 did not show drifts (not shown). We can explain this result, that the surface fields in two experiments are relatively similar, although salinity fields at the 350 m depth are different, by the fact that there can be an infinite number of very different vertical profiles of temperature and salinity that give similar sea-surface-elevation

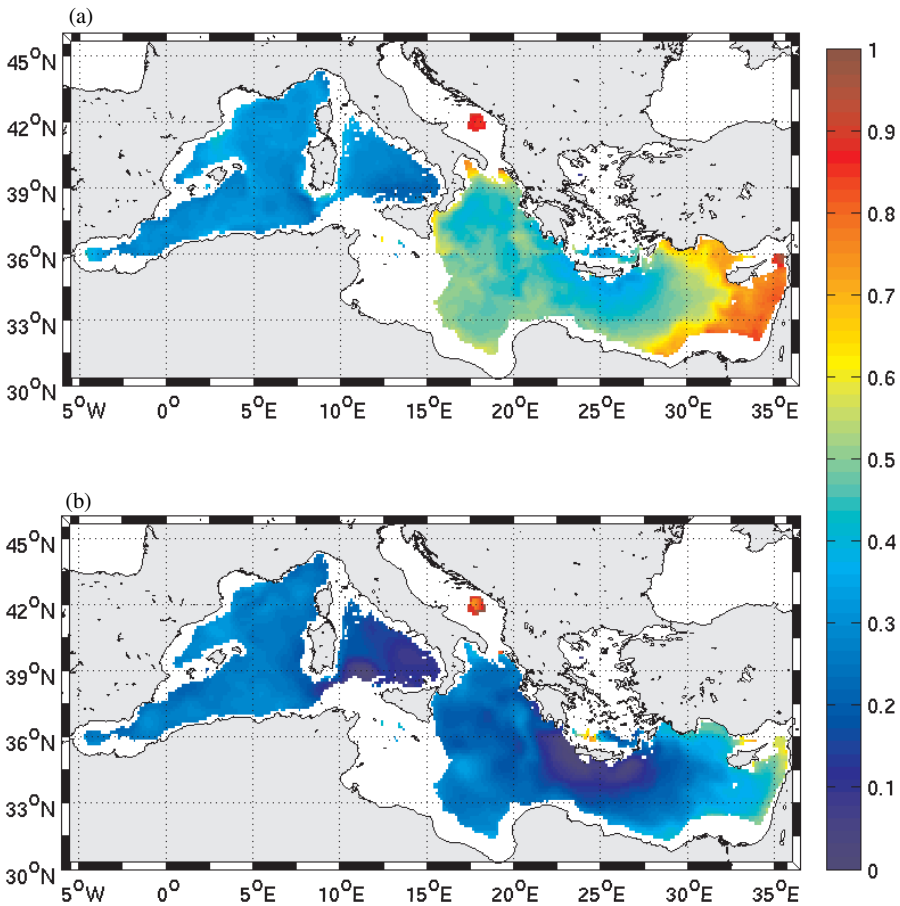


Figure 7. Difference between temperature fields at 1000 m depth simulated by (a) MARK2 and (b) MARK3 in February 2004 and the MEDATLAS winter climatology (degC).

distributions. This can happen because the sea surface elevation depends only on the gradient of the vertical integral of salinity and temperature fields (see (6)) which can be similar for different vertical profiles.

Similarly to the difference in the salinity fields at 350 m depth, a difference was noticed in the temperature field in the deep layers. As an example, Fig. 7 shows the difference between the temperature fields at the 1000 m depth obtained in MARK2 and MARK3 in February 2004 and the winter temperature field from the MEDATLAS climatology (The Medar Group 2002). We can see that, in comparison with MARK2, the use of temporal and spatially variable EOFs in MARK3 significantly reduced the difference between the temperature analysis and the MEDATLAS climatology.

A direct quantitative evaluation of the two assimilation schemes can be obtained by comparing the forecast with independent observations. Figure 8 shows the r.m.s. of residuals of SLA during the period September 1999–December 2002. They are obtained by calculating the difference between SLA fields predicted by the model during 14-day simulations and observed SLA. Residuals are calculated using the first guess at appropriate time method with model SLA fields, which temporally correspond to the time of observations. It is important to notice that observations are compared with

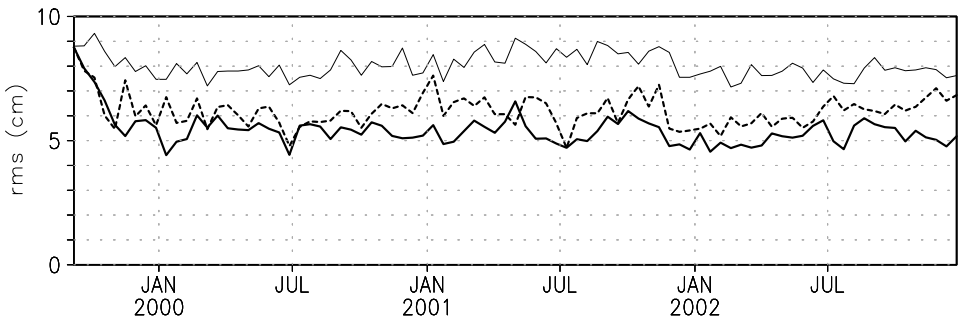


Figure 8. The r.m.s. error (cm) of the SLA predicted by the model. Predicted values are obtained during two-week simulation which start from analyses. The bold dashed line shows results for MARK2, the bold continuous line for MARK3 and the thin continuous line for the run without assimilation.

forecasts before their assimilation and therefore represent an independent dataset for the validation. We can see that in MARK2 the mean r.m.s. of residuals is around 6 cm, while in MARK3 it is around 5.5 cm. In the free run the r.m.s. of the residuals is always higher than with the assimilation scheme, with the mean value of approximately 8 cm, meaning that both schemes improved the prediction of the SLA in comparison with the run without the assimilation.

We have further compared analyses from two experiments with the independent observations which were not assimilated by the system. Independent temperature and salinity observations were taken from ARGO floats positioned in different locations in the Mediterranean in the first six months of 2003, available through the Coriolis Data Center and produced by the Naval Oceanographic Office. Figure 9 shows the r.m.s. of the difference between temperature simulated by the two experiments and observations by ARGO floats. We can see that, in deep layers below 150 m, MARK3 has a much lower r.m.s. error. However, in the first 50 m close to the surface, temperature fields from MARK2 are closer to the observed temperature.

MARK2 predicts more accurately the temperature close to the surface because the single EOF used in MARK2 is set to zero in the top 120 m of the water column, while in MARK3 the temperature correction goes to the surface. As a consequence the surface temperature field in MARK2 is corrected only by SST measurements, and in MARK3 also by SLA measurements. Figure 9 shows that corrections due to SST observations result in a more accurate temperature field close to the surface in comparison with that obtained also from corrections by SLA measurements. This means that MARK3 gives too large a weight to the surface temperature correction due to SLA observations in comparison with the weight due to SST observations.

Figure 9 also shows that in deeper layers, due to the temperature drift, MARK2 is often less accurate than the climatological estimate or the free run without assimilation, although it was always more accurate than the free run for the SLA field (Fig. 8). On the other hand, in deeper layers the temperature field from MARK3 is more accurate than the climatological estimate or the free-run simulation.

Figure 10 shows the r.m.s. error for salinity using the ARGO floats for the comparison. MFS does not assimilate any direct observation of salinity. Therefore, the comparison of predicted and observed salinity provides a completely independent validation of the assimilation system. At almost all depths MARK3 has a smaller r.m.s. error than MARK2, which does not depend significantly on the month. In addition to a relatively large amplitude of the r.m.s. error, MARK2 also shows its relatively large temporal

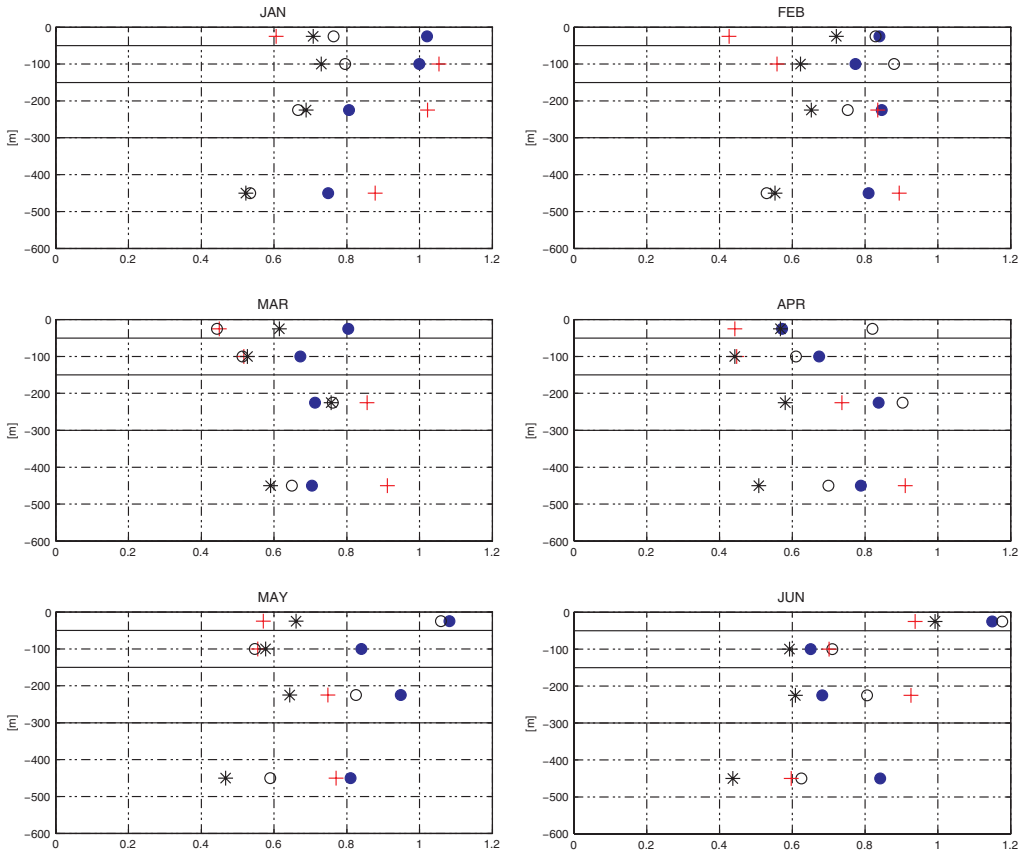


Figure 9. Comparison of the temperature simulated by MARK2 (crosses) and MARK3 (stars) with independent observations by ARGO floats. R.m.s. errors (degC) are grouped in four layers in the vertical, and are shown for the first six months of 2003. Empty circles show the r.m.s. errors for the climatological estimate using the MEDATLAS climatology, and filled circles the r.m.s. errors for the free simulation. In each month the comparison is made using approximately 40 ARGO profiles.

variability. MARK2 has a slightly lower r.m.s. error at the depth of 200 m in April, May and June, but at all other depths and months the r.m.s. error in MARK3 is significantly smaller. Again, due to the salinity drift, MARK2 is often less accurate while MARK3 is always more accurate than the climatological estimate or the free simulation. Furthermore, the comparison with the errors by the climatological estimate or by the free run shows that at the depth of 200 m the higher accuracy of MARK2 in comparison with MARK3 is practically insignificant.

5. DISCUSSION AND CONCLUSIONS

This study presents the changes occurred in the MFS operational system for the assimilation of SLA. A new system MARK3 has been designed and implemented. It uses multivariate time- and space-dependent EOFs in the background-error covariance matrix. The previous operational scheme called MARK2 (Demirov *et al.* 2003) used a single EOF in space and time. Soon after the start of the four-year comparison period we could notice differences between the results of the two assimilation schemes. Generally, MARK3 resulted in a less intensive surface circulation and unlike MARK2 did not show

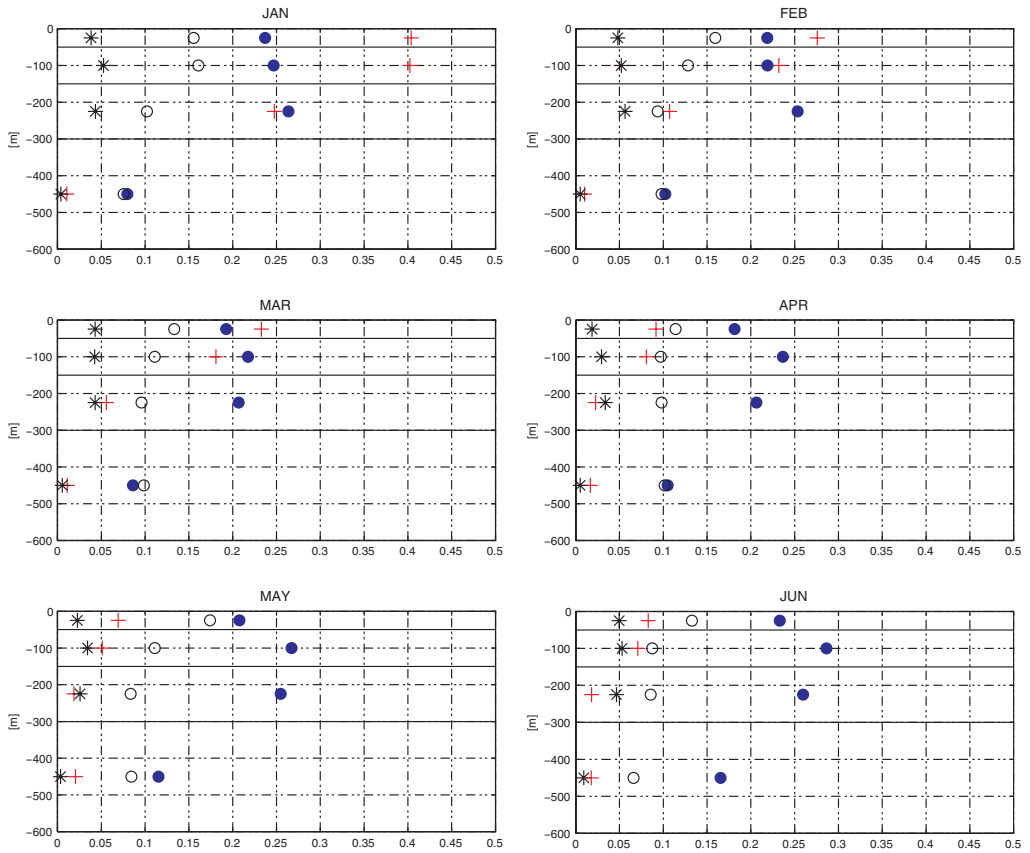


Figure 10. Same as Fig. 9, but for salinity (PSU units).

a major salinity drift. Furthermore, the SLA predicted in MARK3 had a smaller r.m.s. error in comparison with MARK2.

As a confirmation of these results, a comparison with a completely independent dataset of vertical temperature and salinity profiles measured by ARGO floats showed smaller r.m.s. error in MARK3 than in MARK2. Clearly, the use of geographically and seasonally variable EOFs resulted in significantly improved analyses. However, the comparison between MARK2 and MARK3 evidenced that MARK3 corrected the surface temperature field too much using SLA measurements in comparison with the correction by SST measurement. This led to less accurate surface temperature fields obtained in MARK3 in comparison with MARK2. In order to correct this deficiency of the new assimilation scheme, in future it will be necessary to give more weight to the surface temperature correction by SST measurements in relation to the weight of the correction by SLA measurements.

The specification of the background-error correlation matrix in MARK3 can be further refined. For example, we could expect that vertical structures of the error approximately satisfy the geostrophic balance between temperature and salinity error vertical profiles and errors in sea-surface-elevation and stream-function fields (e.g. Daley 1991). A check of the geostrophic balance using (4) showed that some EOFs in MARK3 did not satisfy it (not shown). We are currently investigating how to enforce the approximate

geostrophic balance in the error EOFs and what are the consequences of these changes on the assimilation results.

Another change of the background-error correlation matrix which is currently under development consists in substituting the barotropic stream-function correction with the correction of the full vertical profile of the velocity. In the future we plan to perform analyses each day and update the background-error correlation matrix more frequently. Furthermore, MFS will soon use the same background-error correlation matrix for the assimilation of all observational datasets at once, avoiding the alternating cycle.

Experimental results obtained from the comparison between MARK2 and MARK3 with independent datasets confirm that a more accurate specification of the background-error correlation matrix significantly improves the assimilation results. They suggest that, if other changes in our assimilation system, like increased horizontal and vertical resolution of the numerical model, the improved calculation of surface fluxes, improved assimilation schemes and the assimilation of new datasets will be necessary, further improvements in the calculation of the background-error correlation matrix will represent an important part of the MFS development.

ACKNOWLEDGEMENTS

We would like to thank two unknown reviewers for comments and suggestions. During this study S. Dobricic, M. Adani, A. Bonazzi, C. Fratianni and M. Tonani were supported by the EU project Mediterranean Forecasting System: Toward Environmental Prediction (contract number: EVK3-CT-2002-00075). The work was partially supported by the Italian MIUR FIRB Grid.it project RBNE01KNFP on High Performance Grid Platforms and Tools.

REFERENCES

- Behringer, D. W., Ming, J. and Letmaa, A. 1998 An improved coupled model for ENSO prediction and implications for ocean initialization. Part I: The ocean data assimilation system. *Mon. Weather Rev.*, **126**, 1013–1021
- Castellari, S., Pinardi, N. and Leaman, K. D. 1998 A model study of air–sea interactions in the Mediterranean Sea. *J. Mar. Sys.*, **18**, 89–114
- Daley, R. 1991 *Atmospheric data analysis*. Cambridge atmospheric and space science series, Cambridge University Press, ISBN 0-521-38215-7
- De Mey, P. and Benkiran, M. 2002 'A multivariate reduced-order optimal interpolation method and its application to the Mediterranean basin-scale circulation'. Pp. 281–306 in *Ocean Forecasting*. Eds. N. Pinardi and J. Woods. Springer Verlag, Heidelberg
- Demirov, E. and Pinardi, N. 2002 The simulation of the Mediterranean Sea circulation from 1979 to 1993. Part I: The interannual variability. *J. Mar. Sys.*, **33–34**, 23–50
- Demirov, E., Pinardi, N., Fratianni, C., Tonani, M., Giacomelli, L. and De Mey, P. 2003 Assimilation scheme in the Mediterranean forecasting system: Operational implementation. *Annales Geophysicae*, **21**, 189–204
- Derber, J. C. and Bouttier, F. 1999 A reformulation of the background error covariance in the ECMWF global data assimilation system. *Tellus*, **51A**, 195–221
- Le Traon, P. Y., Nadal, F. and Ducet, N. 1998 An improved mapping method of multisatellite altimeter data. *J. Atmos. Oceanic Technol.*, **15**, 522–533

- Manzella, G., Cardin, V., Cruzado, A., Fusco, G., Gacic, M., Galli, C., Gasparini, G., Gervais, T., Kovacevic, V., Millot, C., Petit DeLa Villeon, L., Spaggiari, G., Tonani, T., Tziavos, C., Velasquez, Z., Walne, A., Zervakis, V. and Zodiatis, G. 2001 EU-sponsored effort improves monitoring of circulation variability in the Mediterranean. *EOS Transactions*, American Geophysical Union, **82**, 497–504
- The MEDAR Group 2002 MEDAR/MEDATLAS 1998–2001 Mediterranean and Black Sea database of temperature, salinity and bio-chemical parameters and climatological atlas (4 CDROMs). www.ifremer.fr/sismer/program/medarIFREMER/TMSI/IDM/SISMER Ed., Centre de Brest, France
- North, G. R., Bell, T. L., Cahalan, R. F. and Moeng, F. J. 1982 Sampling errors in the estimation of Empirical Orthogonal Functions. *Mon. Weather Rev.*, **110**, 699–706
- Pinardi, N. and Masetti, E. 2000 Variability of the large scale general circulation of the Mediterranean Sea from observations and modelling: a review. *Paleogeography, Palaeoclimatology, Palaeoecology*, **158**, 153–173
- Pinardi, N., Rosati, A. and Pacanowski, R. C. 1995 The sea surface pressure formulation of rigid lid models. Implications for altimetric data assimilation studies. *J. Mar. Sys.*, **6**, 109–119
- Pinardi, N., Allen, I., Demirov, E., De Mey, P., Korres, G., Lascaratos, A., Le Traon, P.-Y., Maillard, C., Manzella, G. and Tziavos, C. 2003 The Mediterranean ocean forecasting system: First phase of implementation (1998–2001). *Annales Geophysicae*, **21**, 3–20
- Sparnocchia, S., Pinardi, N. and Demirov, E. 2003 Multivariate Empirical Orthogonal Function analysis of the upper thermocline structure of Mediterranean Sea from observations and model simulations. *Annales Geophysicae*, **21**, 167–187
- Talagrand, O. and Courtier, P. 1987 Variational assimilation of meteorological observations with the adjoint vorticity equation. I: Theory. *Q. J. R. Meteorol. Soc.*, **113**, 1311–1328
- Todling, R. and Cohn, S. 1994 Suboptimal schemes for atmospheric data assimilation based on the Kalman filter. *Mon. Weather Rev.*, **122**, 2530–2557